

Probing turbulent superstructures in Rayleigh-Bénard convection by Lagrangian trajectory clusters

Christiane Schneide,¹ Amrish Pandey,² Kathrin Padberg-Gehle,¹ and Jörg Schumacher^{2,3}

¹*Institut für Mathematik und ihre Didaktik, Leuphana Universität Lüneburg, D-21335 Lüneburg, Germany*

²*Institut für Thermo- und Fluidodynamik, Technische Universität Ilmenau, Postfach 100565, D-98684 Ilmenau, Germany*

³*Tandon School of Engineering, New York University, New York, NY 11201, USA*

(Dated: October 18, 2018)

We analyze large-scale patterns in three-dimensional turbulent convection in a horizontally extended square convection cell by Lagrangian particle trajectories calculated in direct numerical simulations. A simulation run at a Prandtl number $\text{Pr} = 0.7$, a Rayleigh number $\text{Ra} = 10^5$, and an aspect ratio $\Gamma = 16$ is therefore considered. These large-scale structures, which are denoted as turbulent superstructures of convection, are detected by the spectrum of the graph Laplacian matrix. Our investigation, which follows Hadjighasem *et al.*, Phys. Rev. E **93**, 063107 (2016), builds a weighted and undirected graph from the trajectory points of Lagrangian particles. Weights at the edges of the graph are determined by a mean dynamical distance between different particle trajectories. It is demonstrated that the resulting trajectory clusters, which are obtained by a subsequent k -means clustering, coincide with the superstructures in the Eulerian frame of reference. Furthermore, the characteristic times τ^L and lengths λ_U^L of the superstructures in the Lagrangian frame of reference agree very well with their Eulerian counterparts, τ and λ_U , respectively. This trajectory-based clustering is found to work for times $t \lesssim \tau \approx \tau^L$. Longer time periods $t \gtrsim \tau^L$ require a change of the analysis method to a density-based trajectory clustering by means of time-averaged Lagrangian pseudo-trajectories, which is applied in this context for the first time. A small coherent subset of the pseudo-trajectories is obtained in this way consisting of those Lagrangian particles that are trapped for long times in the core of the superstructure circulation rolls and are thus not subject to ongoing turbulent dispersion.

PACS numbers:

I. INTRODUCTION

Compared to investigations of turbulent Rayleigh-Bénard convection in the Eulerian frame of reference [1–3], the number of studies in the Lagrangian perspective in which the turbulent fields and the related transport are monitored along the trajectories of massless point-like particles [4] has remained surprisingly small to date. Numerical studies were primarily focused on the turbulent dispersion of Lagrangian particle pairs [5] and tetrads [6], the entropy production rates along individual Lagrangian trajectories [7] for convection volumes with aspect ratios $\Gamma = L/H \leq 4$ where L is a horizontal extension (side length or diameter). Characteristic turnover times and the geometry of Lagrangian trajectories were analyzed numerically in closed non-rotating [8] and in rotating cells [9, 10]. Laboratory experiments of turbulent convection pioneered the use of smart particles to measure local heat fluxes [11] along individual particle tracks. Complex three-dimensional particle tracking was applied to monitor Lagrangian acceleration statistics [12] and the inhomogeneous flow behavior [13], respectively. The aspect ratios of the convection cells remained below $\Gamma \lesssim 6$ in all these cases. The present study is related to a Lagrangian analysis in a convection flow in a cell with larger aspect ratio of $\Gamma = 16$ for which a large-scale organisation of the turbulent flow is expected.

Recent three-dimensional numerical simulation studies in large-aspect-ratio layers in the Eulerian frame of reference showed that thermal plumes in turbulent convection form a web of connected ridge-like structures of ascending hot (descending cold) fluid from the bottom (top) plate [14]. The corresponding large-scale fluid motion proceeds in form of circulation rolls [15, 16] and the thermal plumes tend to cluster in the course of the dynamical evolution [17, 18]. The characteristic diameter of the large-scale circulation rolls, $\lambda_U/2$, or equivalently the characteristic distance between the strongest adjacent ridges of ascending and descending plumes, $\lambda_\Theta/2$, is a function of Rayleigh and Prandtl number [19–21]. The resulting patterns, which are clearest revealed when a windowed time-averaging is performed in addition, are termed *turbulent superstructures* of convection. These superstructures evolve gradually for times larger than a characteristic time τ which is given by $\tau \sim \ell/u_{\text{rms}}$ with ℓ being the mean circumference of the large-scale rolls and u_{rms} the root mean square velocity [21]. Physically, this time τ is of the order of a typical turnover time of a fluid parcel in a large-scale circulation roll. A Lagrangian analysis of the plume and roll patterns in convective turbulence requires a different approach compared to previous studies in convective turbulence, namely a characterization of the coherent behavior of Lagrangian particles.

Over the last two decades, a number of different concepts have been proposed that describe the notion of Lagrangian coherent behavior. For discussions and comparisons of the major current approaches we refer to refs. [22, 23]. The established approaches can be roughly divided into two different families. (1) *Probabilistic methods* based on transfer operators are tailored to identify finite-time coherent sets as regions that are minimally dispersive over a finite-time span while moving with the flow. For a regularization of the underlying optimization problem diffusion is artificially introduced, so that both advective and diffusive transport are minimized. A uniform description of the different concepts in this framework can be found in [24]. (2) The dynamic objects central to *geometric methods* are Lagrangian coherent

structures (LCS). They are defined as codimension-1 material surfaces that extremise a certain stretching or shearing quantity. Several heuristic diagnostic methods for the identification of LCS such as finite-time Lyapunov exponents (FTLE) but also mathematically sound variational criteria are reviewed in [25]. Whereas LCS form barriers to advective particle transport, the identification of optimal barriers to both advective and diffusive transport has been addressed only very recently in ref. [26]. Finally, another recent geometric characterization [27] defines finite-time coherent sets as sets with minimal boundary to volume ratios under the action of the dynamics. This concept turns out to arise as the advective limit of the probabilistic framework and thus provides an analytical link between the two families of methods.

These established approaches are however less suited for our current study. Here, the aim is to study the emergence and structure of convection rolls, which are macroscopic entities. For this, particles are initialized in a two-dimensional plane near the bottom plate in a three-dimensional convective flow. Whereas the geometric approach will identify the detailed turbulent skeleton including the small-scale structures such as vortices (see an FTLE-analysis in Sect. III.C; we also refer to [28] for a study of a three-dimensional turbulent shear flow), the probabilistic framework – although tailored for targeting large-scale structures in general – is not immediately applicable either due to the two-dimensional seed of particles. Thus, an approach is required that can identify large-scale coherent behavior directly from the given Lagrangian trajectory data. Recent promising works make use of spatio-temporal clustering algorithms applied to Lagrangian trajectory data [29–33], where the aim is to identify coherent sets as groups of trajectories that remain close and/or behave similarly in the time span under investigation.

Here, our focus will be on the latter approaches. In particular, we apply spectral graph theory [34, 35] and, for the first time in this context, the algorithm known as density-based spatial clustering applications with noise (DBSCAN) [36] to analyze the time evolution of a Lagrangian particle ensemble as a whole. To this end, the particle trajectories are composed to a network and its connection to the large-scale organization of a three-dimensional turbulent convection flow at large aspect ratio is studied. The set of N_p individually advected Lagrangian particles at a time t forms a set of vertices $\{v_1, \dots, v_{N_p}\} \in V$ of a weighted and undirected graph $G = (V, E, w)$. The vertices are connected by edges $\{e_1, \dots, e_M\} \in E$. The dynamical history of the particle ensemble up to time t is encoded in weights w which are assigned to each edge. Our applied trajectory analysis follows in their steps the one of Hadjighasem *et al.* [30] for Lagrangian vortex detection. The weights are calculated as the inverse of a time-averaged distance of mutual tracer trajectories and set to zero if this distance exceeds a threshold value. The latter is the sparsification step. By solving a balanced cut problem via an equivalent generalized eigenvalue problem of the Laplacian matrix of the graph [37], the network is decomposed into k subgraphs or clusters. We relate the obtained clusters of the graph to superstructure rolls of the turbulent convection flow. The dispersion of the Lagrangian particles that start their evolution in close distance to each other is an immanent property of a turbulent flow and can be quantified by the largest Lyapunov exponent. The standard spectral clustering analysis is applicable for the shorter-time evolution only, i.e., for time intervals $t \lesssim \tau$. We will compare the results to the corresponding finite-time Lyapunov exponent field, which measures local separation over a finite-time horizon. For times $t \gtrsim \tau$, a density-based clustering [36] of pseudo-trajectories, which are obtained as time averages of Lagrangian trajectories, will be applied to probe the long-living turbulent superstructures. The latter analysis step gives us the most coherent subset of trajectories which are trapped for a long time in the core of the circulation rolls.

Spatio-temporal clustering of Lagrangian particle trajectories has been applied recently for several flows with dominating vortex structures, such as a Bickley jet on a plane [30–32], two-dimensional polar vortex flow [33], point vortex flows [38], and two-dimensional box turbulence with an inverse energy cascade [23, 39]. The present work comprises an application of such an analysis to a complex three-dimensional turbulent convection flow in an extended domain and the first use of DBSCAN in this context. Our main objective in this work is rather to apply these concepts for a Lagrangian analysis of turbulent superstructures in one example than to present comprehensive parameter studies at higher Rayleigh numbers or even larger aspect ratios, which are left for the future.

In the following Sec. II, we will summarize the numerical method and the basics of the applied graph theory. In Section III we will determine the characteristic scales of the superstructures in the Lagrangian frame of reference, report our results on the short-term analysis for times $t \lesssim \tau$ and the long-term analysis for $t \gtrsim \tau$. We conclude the work with a summarizing discussion in Sec. IV and give a brief outlook.

II. METHODS

A. Boussinesq approximation and numerical model

We solve the three-dimensional equations of motion of turbulent convection in the Boussinesq approximation for which the fluid mass density is a linear function of the temperature. The equations are made dimensionless by using height of the cell H , the free-fall velocity $U_f = \sqrt{g\alpha\Delta TH}$ and the imposed temperature difference ΔT . Times are

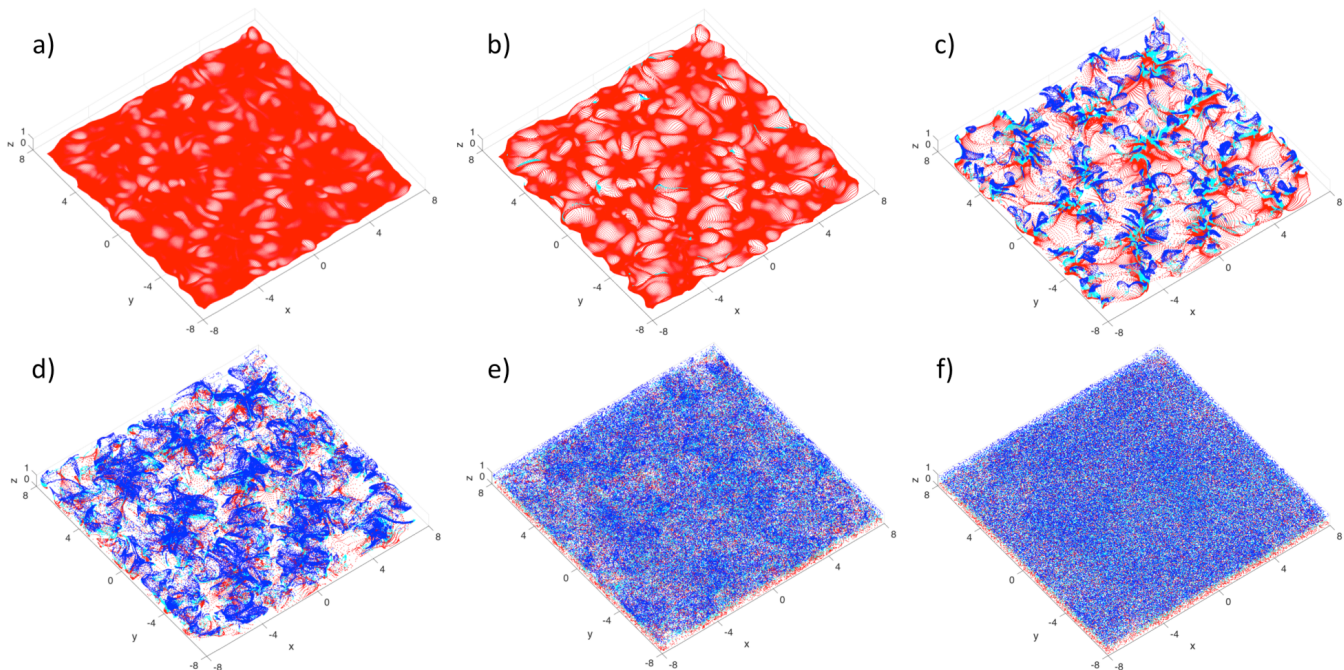


FIG. 1: Lagrangian tracer particle distributions in the turbulent convection cell at different times. Tracers with a vertical position of $0 \leq z < H/3$ are colored in red, $H/3 \leq z < 2H/3$ in cyan, and $2H/3 \leq z \leq H$ in blue. Times in free-fall time units are $t = 1.3 T_f$ in (a), $2.6 T_f$ in (b), $6.5 T_f$ in (c), $10.4 T_f$ in (d), $30.1 T_f$ in (e), and $49.8 T_f$ in (f).

expressed in units of the free-fall time $T_f = H/U_f$. The equations are given by

$$\nabla \cdot \mathbf{u} = 0, \quad (1)$$

$$\frac{\partial \mathbf{u}}{\partial t} + (\mathbf{u} \cdot \nabla) \mathbf{u} = -\nabla p + \sqrt{\frac{\text{Pr}}{\text{Ra}}} \nabla^2 \mathbf{u} + T \mathbf{e}_z, \quad (2)$$

$$\frac{\partial T}{\partial t} + (\mathbf{u} \cdot \nabla) T = \frac{1}{\sqrt{\text{RaPr}}} \nabla^2 T, \quad (3)$$

with Rayleigh and Prandtl numbers that are given by $\text{Ra} = g\alpha\Delta TH^3/(\nu\kappa)$ and $\text{Pr} = \nu/\kappa$. No-slip boundary conditions for the fluid ($\mathbf{u} = 0$) are applied at all walls. The side walls are thermally insulated ($\partial T/\partial \mathbf{n} = 0$) and the top and bottom plates are held at constant dimensionless temperatures $T = 0$ and 1 , respectively. These specific side wall boundary conditions are taken in order to be able to compare the results to laboratory experiments which are currently in progress. In the following, we consider the case of $\text{Ra} = 10^5$, $\text{Pr} = 0.7$ and $\Gamma = 16$. The simulation data are generated by the spectral element method nek5000 [40, 41] with 441,000 spectral elements and a polynomial expansion up to 5th order which is parallelized with respect to all three space dimensions. The mean turbulent heat transfer is measured by the Nusselt number which is given by $\text{Nu} = 1 + \sqrt{\text{RaPr}} \langle u_z T \rangle_{V,t} = 4.1$, where the average of the heat flux is taken with respect to the whole domain V and total time t .

Lagrangian tracer particles are seeded into the simulation domain on a regular mesh with $N_p = 512^2$ points at a height of $z = 0.03$ above the bottom plate which is well inside the thermal boundary layer that has a mean thickness $\delta_T = 1/(2\text{Nu}) = 0.121$. Each individual tracer particle is advected corresponding to

$$\frac{d\mathbf{X}_i}{dt} = \mathbf{u}(\mathbf{X}_i, t), \quad (4)$$

with $i = 1 \dots N_p$. The interpolation of the velocity field to the tracer position can be done spectrally in the present simulation code and is thus as accurate as the spectral expansion of the Eulerian fields itself. Time advection of tracers is done by a two-step Adams-Bashforth method. Figure 1 displays the tracer distribution at different instants. Initially, the Lagrangian particles accumulate in regions of rising thermal plumes (see panels (a–c)) and are advected to the top plate where they separate hyperbolically (see panel (d)) and move downward again, either in the same circulation roll or in different rolls. With progressing time tracer particles fill the whole convection layer as visible in panels (e,f). In the perspective view they appear as a well-mixed cloud that contains no more information about the large-scale patterns of the advecting flow. Our following analysis will show that information on the advecting flow structures is still obtainable from the tracer ensemble.

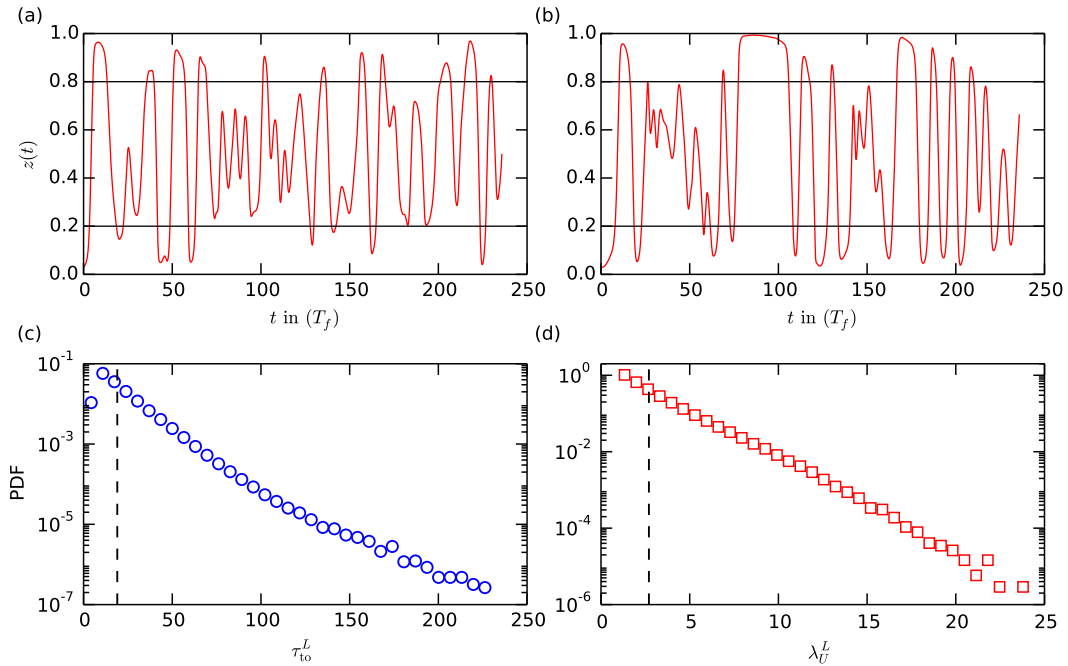


FIG. 2: Characteristic Lagrangian times and scales of turbulent superstructures. (a,b) Typical Lagrangian particle tracks showing the vertical particle coordinate $z(t)$ for individual tracers no. 2 in (a) and no. 2045 in (b). The horizontal lines at $z = 0.2$ and $0.8H$ in both panels indicate the heights that were used to determine the Lagrangian turnover times. (c) Probability density function (PDF) of Lagrangian turnover time τ_{to}^L . The dashed vertical line indicates the mean Lagrangian turnover time $\bar{\tau}_{to}^L = (19.1 \pm 12.8)T_f$. The root mean square (rms) value from this statistics is $23.0T_f$. (d) PDF of the characteristic Lagrangian scale λ_U^L . The vertical line indicates again the mean with $\bar{\lambda}_U^L = (2.7 \pm 0.9)H$. This stands for the diameter of a pair of rolls. The rms value is $3.2H$.

B. Spectral analysis of Lagrangian tracer network

In correspondence with [30] the trajectory cluster analysis comprises the following steps: (i) graph construction from the trajectory points, (ii) determination of the weights at the edges, (iii) sparsification of the graph, (iv) solution of the generalized eigenvalue problem of the graph Laplacian matrix and determination of the gap in the ordered eigenvalue spectrum, and (v) cluster detection by k -means clustering where k indicates the first pronounced gap in the spectrum. The N_p Lagrangian particle trajectories $\mathbf{X}_i(t)$ are sampled at discrete time instances $t_k = \{0, 1, \dots, N_t\}\Delta t$. This information enters the construction of an undirected, weighted network with $n = N_p$ nodes or vertices. The weight w_{ij} of the link between nodes i and j depends on the time-averaged distance r_{ij} between the nodes [30] which is given by

$$r_{ij} = \frac{1}{N_t \Delta t} \int_0^{N_t \Delta t} |\mathbf{X}_i(t) - \mathbf{X}_j(t)| dt = \frac{1}{w_{ij}}. \quad (5)$$

The weights thus contain the mutual trajectory histories up to $t = N_t \Delta t$ as an accumulated measure. A network with n vertices has $M = n(n-1)/2$ edges if every node or vertex is connected with every other node. Self-connections are excluded. In order to sparsify the network (and thus the related adjacency or similarity matrix), we only consider links with weight $w_{ij} > 1/\epsilon$ with $\epsilon > 0$. This network can be uniquely described by the similarity matrix $W \in \mathbb{R}^{n,n}$ with

$$W_{ij} = \begin{cases} w_{ij}, & i \neq j, r_{ij} < \epsilon \\ 0, & \text{else} \end{cases}. \quad (6)$$

The choice of ϵ is discussed later in the text in Section III. The degree matrix D , given by $D_{ii} = \sum_{j=1}^n W_{ij}$, is a diagonal matrix with node degrees $d_i = D_{ii}$ as entries. It can be used to calculate the non-normalized graph Laplacian $L = D - W$. As shown by Shi and Malik [37], the solution of the generalized eigenvalue problem

$$Lv = \lambda Dv, \quad (7)$$

serves as indicator for the subdivision of the graph into clusters. The eigenvalues are non-negative and real, $0 = \lambda_1 \leq \lambda_2 \leq \dots \leq \lambda_n$, with the corresponding eigenvectors v_1, \dots, v_n . In particular, the eigenvector corresponding to the second smallest eigenvalue of (7) approximates the solution of the normalized cut (Ncut) problem introduced by [37] which seeks to minimize the connectivity between clusters while maximizing simultaneously the connectivity within

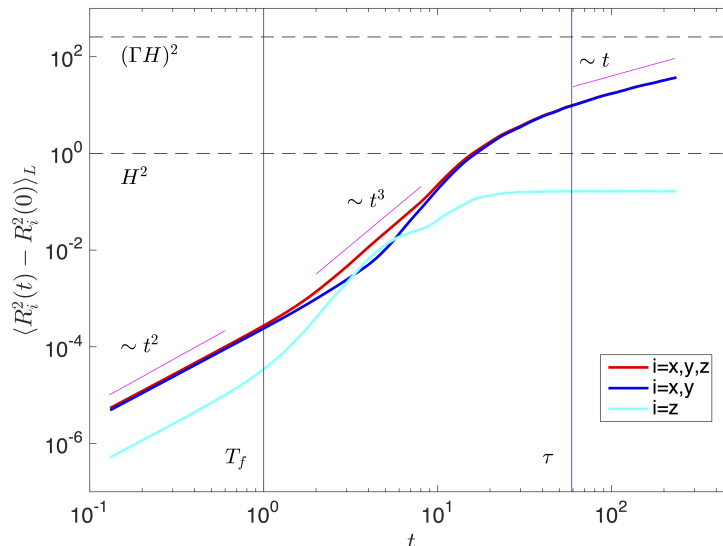


FIG. 3: Lagrangian tracer pair dispersion versus time. Ballistic, Richardson-like intermediate and diffusive scaling are indicated in addition to all relevant times and outer scales in the problem. The total dispersion is shown together with its two contributions, the vertical and horizontal pair dispersions. Times are given in units of the free-fall time $T_f = H/U_f$, pair dispersion in units of H^2 . Again $\tau \approx \tau^L$.

clusters. Eigenvectors corresponding to the next smallest eigenvalues can be used to further subdivide the graph. The number of leading eigenvalues close to zero determines the number of nearly decoupled communities in the network [43, 44]. Such nearly decoupled subgraphs correspond to bundles of trajectories that are internally well connected but only loosely tied to other trajectories, an indication of coherent behavior (see also [30]). We apply a k -means clustering algorithm on the eigenvectors corresponding to the k leading eigenvalues in order to extract k clusters [45]. The number of leading eigenvalues is determined by a spectral gap heuristics.

III. RESULTS

A. Characteristic time and length scales of large-scale patterns in Lagrangian frame

The first question to answer is the one on the agreement of the characteristic pattern scales in the Eulerian and Lagrangian frames of reference. Both, the characteristic time and length scales are of central interest for a separation of the fast, small-scale from the gradual, large-scale dynamics. In correspondence with [21], we determined the characteristic time of the turbulent superstructures in the Eulerian frame of reference with $\tau \approx 3\ell/u_{\text{rms}} = 59T_f$ for the present data set. The characteristic Eulerian length scale of the temperature patterns was determined to $\lambda_\Theta = 4$, either by a Fourier analysis or the evaluation of the spatial correlations. The scale of a pair of counterrotating circulation rolls, λ_U , was of comparable size.

Here, the large-scale structure can be probed directly on the basis of the Lagrangian particle tracks. The analysis is summarized in Fig. 2. Panels (a) and (b) display the vertical coordinate of two typical Lagrangian particle tracks. As visible, the tracers do not follow a perfect upwelling-downwelling motion, remain partly trapped close to the top or bottom plates as well as in the center of the convection layer. We measure the turnover time for each individual Lagrangian particle as the time it takes to rise from heights $z < 0.2$ to $z > 0.8$ and back down again. These heights are slightly above and below the lower and upper thermal boundary layers, respectively. Recall again that the thermal boundary layer thickness is $\delta_T = 0.121$. The corresponding probability density function (PDF) of the Lagrangian turnover time τ_{to}^L is given in Fig. 2(c). The PDF is characterized by a fat (stretched exponential) tail that implies the high probability of long excursions of the Lagrangian tracer particle in the bulk. The mean value is found to be $\bar{\tau}_{\text{to}}^L = (19.1 \pm 12.8)T_f$ and thus agrees very well with the Eulerian analysis, $\tau/3 \approx 19.7T_f$. It can now also be seen that the prefactor of 3, which we have chosen in the Eulerian analysis in [21], is justified by the tail of the distribution. Turnovers can take as long as $200 T_f$ and even more. In ref. [21], it was shown that somewhat smaller or larger prefactors than 3 lead to very similar results. We conclude that

$$\bar{\tau}_{\text{to}}^L \approx \frac{1}{3}\tau \quad \text{and thus} \quad \bar{\tau}^L \approx \tau \quad (8)$$

follows consistently from our analysis.

For the calculation of a characteristic spatial scale in the Lagrangian frame, we take the midplane of the convection layer at $z = 0.5$ and determine the distance of the points of subsequent rising and falling events of each Lagrangian particle track. This distance corresponds to $\lambda_U^L/2$ since the wavelength is taken for a pair of circulation rolls. The corresponding distribution is plotted in Fig. 2(d). Again, we detect an exponential tail that suggests a wide range of possible scales. The mean value is $\bar{\lambda}_U^L = (2.7 \pm 0.9)H$. This number is a bit smaller than the Eulerian value of 4 which can be attributed to trajectories that get trapped in the core regions of the superstructure rolls for longer times. The large variability is seen from the error bar in the mean values. We conclude that

$$\bar{\lambda}_U^L \lesssim \lambda_U \quad (9)$$

follows from our analysis and that both scales of the superstructures consistently match with their Eulerian counterparts.

In section II B we introduced already the parameter ϵ for the sparsification of the graph which is associated with the time-averaged distance between Lagrangian trajectories. We have chosen a value of $\epsilon = 0.75$ throughout our analysis. In the absence of a rigorous criterion for the choice of this parameter, we provide physical arguments in the following. The cut parameter ϵ should be bounded from below by the thermal boundary layer thickness δ_T which is comparable to the width of the stems of detaching line-like thermal plumes [46]. In a rising (or falling) thermal plume two Lagrangian particles will display a correlated upward (or downward) motion. The thickness of the thermal boundary layer varies locally and forms a distribution with δ_T as the mean. As shown in ref. [42], such a local boundary layer thickness distribution has typically an extended tail to larger scales. Furthermore the thermal plumes disperse as they move to the bulk. This causes an additional increase of their thickness. On the large-scale end, the cut parameter ϵ should be bounded from above by $\lambda_\Theta/2 \approx \lambda_U/2$, which is about 2 in our case at hand.

B. Connection to Lagrangian particle pair dispersion

It is interesting to relate the detected time scale $\tau \approx \tau^L$ of the superstructures to the Lagrangian particle pair dispersion. All particle pairs had the same initial separation of $R_0 = 0.005$. The pair dispersion is defined as the mean square of the particle pair distance, the latter of which is given by $\mathbf{R}(t) = \mathbf{X}_1(t) - \mathbf{X}_2(t)$. It can be decomposed into a horizontal and vertical contribution [6]

$$\mathbf{R}^2(t) = \mathbf{R}_{xy}^2(t) + R_z^2(t)e_z. \quad (10)$$

In Fig. 3 we display the pair dispersion $\langle \mathbf{R}^2(t) - \mathbf{R}_0^2 \rangle_L$ versus time with $\mathbf{R}_0^2 = \mathbf{R}^2(0)$. The symbol $\langle \cdot \rangle_L$ stands for an average over all N_p trajectories. Times $t \lesssim T_f$ are characterized by the ballistic separation of tracers within a pair. This follows by a Taylor expansion and results in a scaling of $\langle \mathbf{R}^2(t) - \mathbf{R}_0^2 \rangle_L \sim t^2$. For $t \gtrsim 10T_f$ the vertical pair dispersion $\langle R_z^2(t) - R_{z,0}^2 \rangle_L$ saturates to a constant that is smaller than H^2 . In a crossover period between $t \sim T_f$ and $10 T_f$, the total pair dispersion follows a Richardson-type scaling that grows with t^3 . It is the horizontal dispersion $\langle \mathbf{R}_{xy}^2(t) \rangle_L$ that eventually takes over and dominates the long-time behavior. The long-time limit of the pair dispersion is the diffusion limit for which $\langle \mathbf{R}_{xy}^2(t) \rangle_L \sim t$ [47]. Figure 3 shows clearly that the beginning of this regime coincides with the characteristic time scale of the turbulent superstructures, τ . From the perspective of an individual Lagrangian tracer particle, the motion within a particle pair is then almost decorrelated and requires an additional clustering. In the following, we conduct the network analysis in respect of the determined time scale and divide it into a short-term ($t \lesssim \tau$) and long-term ($t \gtrsim \tau$) trajectory clustering.

C. Short-term evolution of the Lagrangian network

Figure 4 summarizes our spectral graph analysis for times $t \lesssim \tau^L$. All particles start inside the thermal boundary layer at a distance $z \approx \delta_T/4$ from the bottom wall. Panels (a)–(c) show the temperature at the midplane $z_0 = 1/2$ which is successively longer time-averaged for three different time intervals $N_t \Delta t$ in correspondence with

$$\Theta(x, y, z_0; N_t \Delta t) = \frac{1}{N_t \Delta t} \int_0^{N_t \Delta t} T(x, y, z_0, t') dt'. \quad (11)$$

This definition of the time-averaged temperature is similar to the one used in ref. [21]. The characteristic scale of the turbulent superstructures of the temperature field T which is denoted as λ_Θ is indicated in Fig. 4(c).

The two lower rows of Fig. 4 display the results of the spectral analysis and the subsequent clustering for these times. The cut-off parameter $\epsilon = 0.75$. Panels (d)–(f) depict the different clusters. We plot the initial position of the Lagrangian particles that belong to the same cluster in the same color. The background texture stands for the field of the maximum FTLE advanced over the same time interval [25]. The FTLE for some initial particle position $\mathbf{X}_0 = \mathbf{X}(0)$ over the time span $[0, N_t \Delta t]$ (i.e. $t = N_t \Delta t$) is defined as

$$\sigma_t(\mathbf{X}_0) = \frac{1}{2N_t \Delta t} \ln \lambda_{\max}(\Phi_t(\mathbf{X}_0)), \quad (12)$$

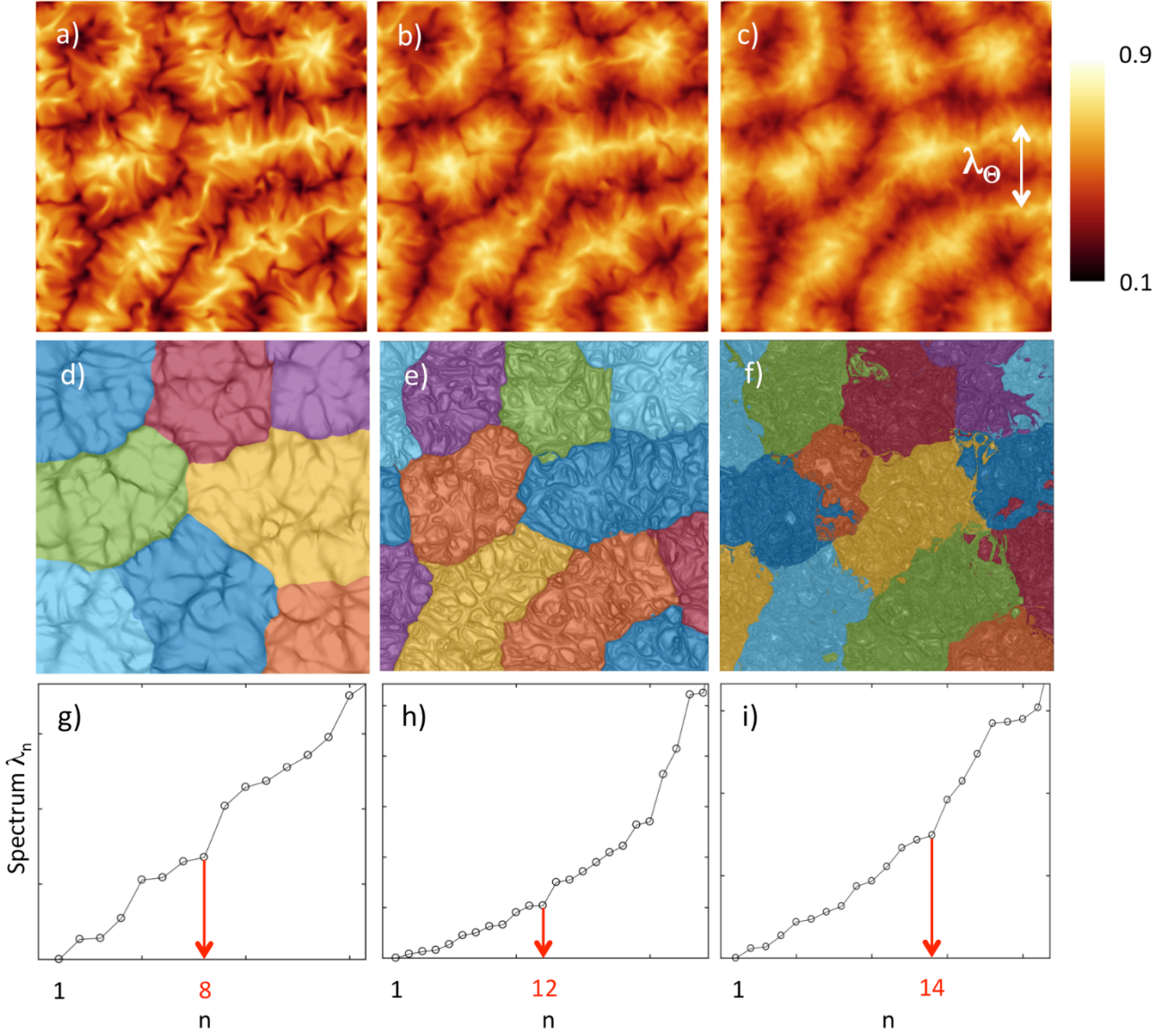


FIG. 4: Time evolution of the Lagrangian superstructures. (a–c) Time-averaged temperature field in the midplane. Averaging times are $N_t \Delta t = 2.6, 10.4,$ and 30.1 free-fall time units, respectively. In panel (c), the characteristic scale λ_Θ of the turbulent superstructures is indicated by a double arrow. (d–f) Lagrangian trajectory clusters obtained from the leading eigenvectors of the graph Laplacian. Particles that belong to the same spectral cluster at time $N_t \Delta t$ are colored equally. The background contours are the ridges of the maximum finite-time Lyapunov exponent (12). Ridges and clusters are indicated with respect to the initial Lagrangian particle position. (g–i) Corresponding eigenvalue spectra of the graph Laplacian. The spectral gap between eigenvalues no. 8–9, 12–13, and 14–15 is used to detect $k = 8, 12,$ and 14 trajectory clusters by the k -means clustering algorithm, respectively. The cut-off parameter is $\epsilon = 0.75$.

where

$$\Phi_t(\mathbf{X}_0) := \left(\frac{d}{d\mathbf{X}_0} \mathbf{X}(t) \right)^T \cdot \frac{d}{d\mathbf{X}_0} \mathbf{X}(t). \quad (13)$$

denotes the Cauchy-Green strain tensor and λ_{\max} the largest eigenvalue of this tensor.

While the FTLE field initially picks up isolated structures that appear to be the signature of the boundaries between convection roles (cf. [48]), it displays ever finer textures with increasing time while the cluster number remains almost the same. At early times, the FTLE ridges coincide partly with the cluster boundaries. The best agreement of the cluster boundaries and most prominent FTLE ridges is achieved for the time interval of 10.4 free-fall time units, panel (e). Panels (g)–(i) of the same figure show the eigenvalue spectra of the graph Laplacian matrix L at the corresponding time and highlight the spectral gap that suggests the segmentation into k clusters by a k -means clustering algorithm [45]. The resulting trajectory clusters agree rather well with the appearing Eulerian superstructure patterns. This can be seen by a comparison of the first and second rows of Fig. 4. However, the trajectory clusters become increasingly

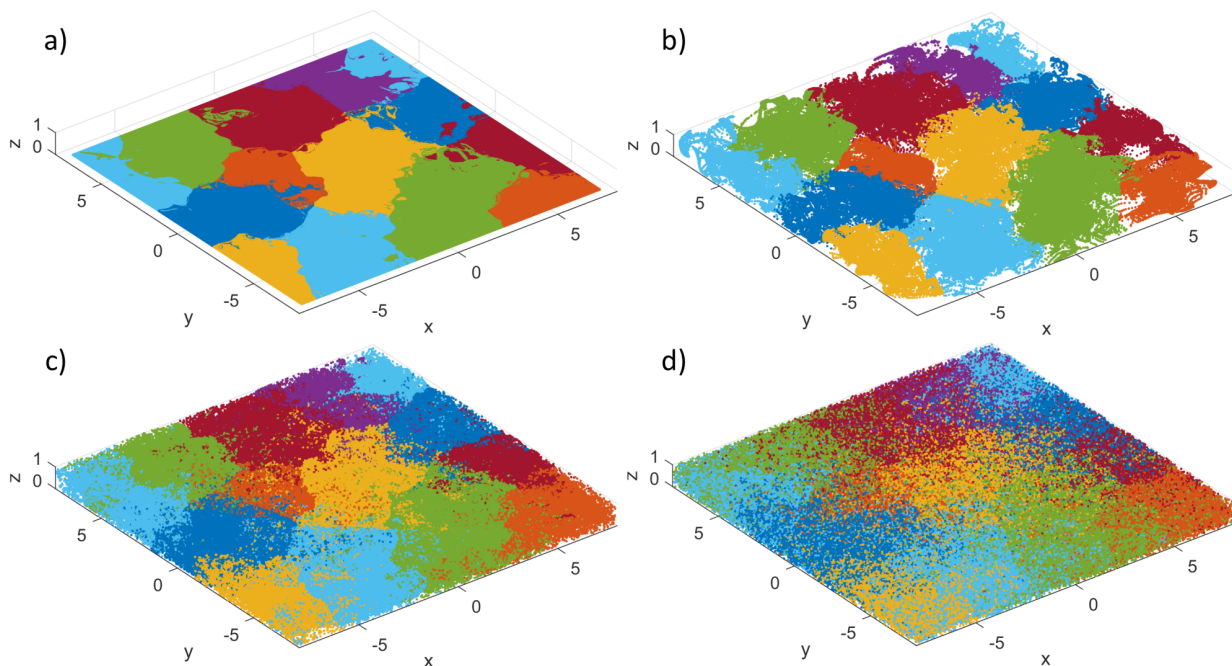


FIG. 5: Perspective view of the whole Lagrangian tracer ensemble at times $t = 0T_f$ in (a), $10.4 T_f$ in (b), $30.1 T_f$ in (c), and $69.4 T_f$ in panel (d). The particles are colored with respect to their trajectory cluster membership as computed for the case $N_t\Delta t = 30.1 T_f$ (cf. Fig. 4 (f)).

fragmented as the monitoring time $N_t\Delta t$ approaches τ^L (not shown). Turbulent dispersion separates an increasing fraction of pair trajectories as time progresses. This eventually also limits the trajectory-based clustering algorithm.

The temporal evolution of the Lagrangian tracers within the clusters is displayed in Fig. 5. We show perspective plots of the full tracer ensemble at four different times, $N_t\Delta t = 0, 10.4, 30.1$ and $69.5 T_f$. In all four panels of this figure we color each Lagrangian tracer with respect to the trajectory cluster that was identified for the averaging time $N_t\Delta t = 30.1 T_f$ (see also Fig. 4 (f)) for this particle. The figure demonstrates that the majority of the Lagrangian tracers stay in the cluster up to times $t = 30.1 T_f$. Panel 5(d) shows in addition that even for more than twice this time (and $t \simeq \tau$) the coarse structure of the clusters is still identifiable although a significant amount of the Lagrangian particles has been transported to other phase space regions due to turbulent dispersion.

We carried out the same analysis using different ϵ and different numbers of tracer particles, respectively, leading to similar results for the number and distribution of clusters (not shown).

D. Long-term evolution by density-based clustering of pseudo-trajectories

The long-term evolution for times $t \gtrsim \tau^L$ requires the construction of pseudo-trajectories from the Lagrangian particle tracks which will be described in the following. Lagrangian pseudo-trajectories are defined as

$$\bar{\mathbf{X}}(n\hat{\tau} + \tau_{\text{to}}^L) = \frac{1}{\bar{\tau}_{\text{to}}^L} \int_{n\hat{\tau}}^{n\hat{\tau} + \bar{\tau}_{\text{to}}^L} \mathbf{X}(t') dt'. \quad (14)$$

with $n = 0, 1, \dots, n_{\text{end}}$ and $\hat{\tau} = 1.31T_f$ (which corresponds to 200 integration time steps). It turns out that we have to apply here again a coarse-graining procedure to reveal the superstructures. In a nutshell, the time average of the turbulence fields in the Eulerian case corresponds with the time average of the pseudo-trajectories in the Lagrangian frame of reference. The time scale $\bar{\tau}_{\text{to}}^L$ is the mean turnover time of a Lagrangian particle in a superstructure roll as determined in Sec. III A. In free-fall time units, we therefore take $\tau_{\text{to}}^L \approx \tau = 19.7T_f$ for the given set. The time-averaged position of a Lagrangian particle should thus coincide for 19 to 20 T_f with the center of a superstructure roll. Many trajectories will not meet this stringent selection procedure due to the ongoing turbulent dispersion of particles that have been originally closely together. Figure 6 displays the time evolution of four individual Lagrangian trajectories together with their corresponding pseudo-trajectories for a time interval $t/T_f \in [0, 80]$. Clearly visible is that the pseudo-trajectories are found indeed in the bulk of the convection layer (see again panels 6 (e,f)).

Based on the obtained pseudo-trajectories, we apply the DBSCAN algorithm by Ester *et al.* [36]. Considering a set of points D , DBSCAN evaluates the ϵ -neighborhood of each point in the set D . A core point P of a cluster \mathcal{C} is a point whose ϵ -neighborhood contains at least MinPts points, thus determining a density in the data space. All points in the ϵ -neighborhood of P are assigned to cluster \mathcal{C} . They can be core points such as point P itself or border points of the

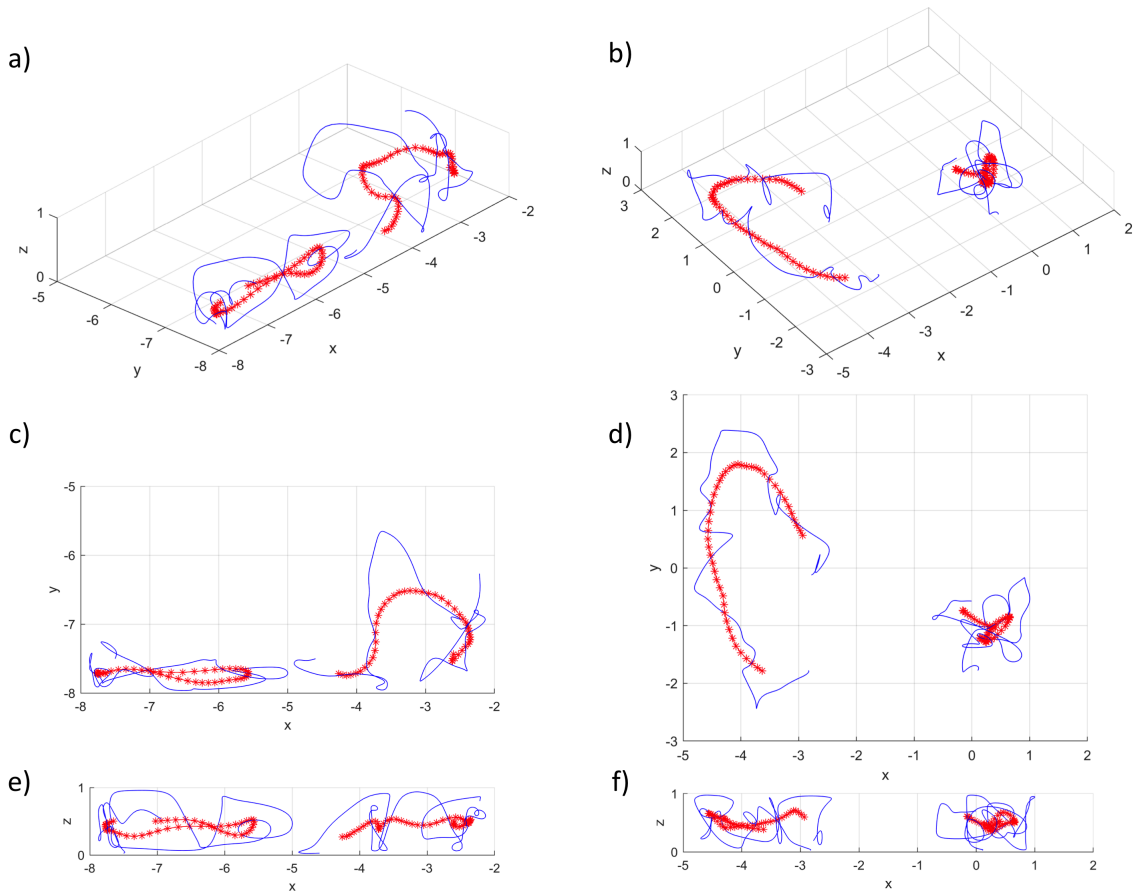


FIG. 6: Time evolution of four individual trajectories (in blue) and their corresponding pseudo-trajectories (in red) plotted for the time interval $t/T_f \in [0, 80]$. The asterisks at the pseudo-trajectories indicate the positions $\bar{\mathbf{X}}(n\hat{\tau})$ for n integer. Two trajectories are displayed in a three-dimensional perspective (panel (a)) and in two projections in panels (c,e). The same sequence follows for another set of two trajectories in panel (b) and panels (d,f), respectively.

cluster. The number of points in the ϵ -neighborhood of border points of a cluster is smaller than the limit MinPts . Subsequently, this process is repeated for all core points of cluster \mathcal{C} . The set of points in the database which are not assigned to any cluster is defined as noise. We extend this algorithm to our spatio-temporal dataset by interpreting the pseudo-trajectories as points and using the dynamical distance r_{ij} as distance function.

The resulting clustering into dense regions (clusters) and sparse regions (noise) for different integration times $T_{\text{end}} = n_{\text{end}}\hat{\tau} + \tau_{\text{to}}^L$ using a value of $\text{MinPts} = 500$ is summarized in Fig. 7 and Table I. We will take again $\epsilon = 0.75$ as in section III C for the short-term analysis. The plots show the midpoints of the pseudo-trajectories, $n \approx n_{\text{end}}/2$, according to the clustering in blue (dense regions) or red (sparse regions) over the time-averaged temperature field in midplane in gray. The number of noisy pseudo-trajectories increases with increasing time. These trajectories contribute to transport in the system as they mingle extensively with other trajectories during the considered time interval and move up- and downward.

The density arising from the chosen combination of the parameters ϵ and MinPts is too small to distinguish between mixing and non-mixing trajectories for the selected shortest time interval of $40T_f$, as seen in the first row of Table I. We have found that in this case an increase of MinPts to 1000 leads to the detection of ~ 2450 noisy trajectories which is still less than 1 per cent of the total number of N_p trajectories. Only for times $t > \tau^L$, the number of noisy trajectories grows. Compared to trajectories in dense regions, which cluster between adjacent ridges of thermal plumes, noisy trajectories primarily assemble at ridge positions as seen in panels (b)–(d) and (g)–(i) of Fig. 7. The noisy trajectories are thus found exactly where the strongest up- or downwelling motion and a subsequent trajectory separation is present.

We conclude furthermore that the detected clusters are trajectories that remain trapped within the superstructure circulation rolls for a considerable part of the examined time interval. The DBSCAN algorithm detects thus exactly those pseudo-trajectories that contribute least to the transport. For even longer times, $t \gtrsim 2\tau$, the analysis in the present case is affected by the side wall boundary conditions and thus stopped. This is seen in panel (e) of Fig. 7 where the trajectories cluster at the side walls. We suspect that this effect will be absent when periodic boundary conditions at the side walls are used. We leave this specific task for our future work.

Time T_{end} (in T_f)	No. of pseudo-trajectories in dense regions	No. of clusters
40	262112	1
60	255047	1
80	210345	1
100	105551	29
120	17601	12

TABLE I: Results of the DBSCAN clustering for different time spans in units of the free fall time T_f . The threshold value that determines the ϵ -neighborhood of a trajectory was chosen to $\epsilon = 0.75$. The threshold to obtain a cluster was set in the analysis to $\text{MinPts} = 500$.

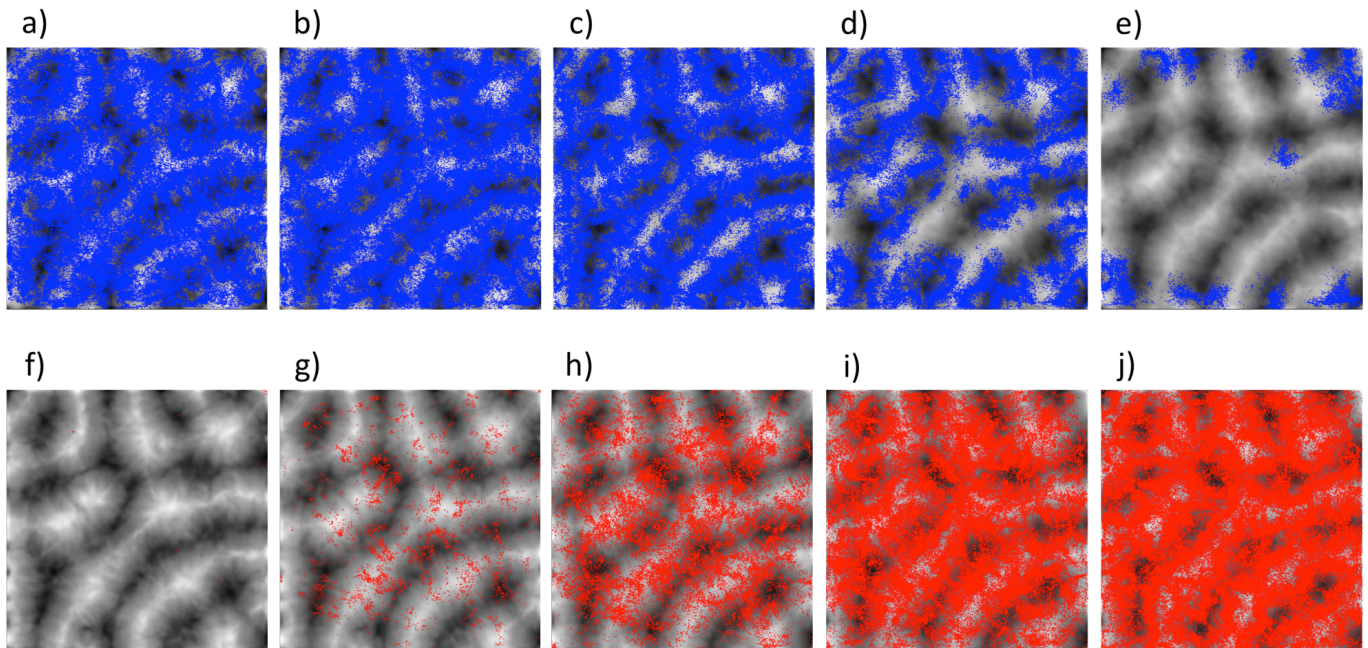


FIG. 7: Time evolution of the Lagrangian pseudo-trajectories for total integration times $T_{\text{end}} = 40T_f \approx 2\tau^L/3$ (a,f), $60T_f \approx \tau^L$ (b,g), $80T_f \approx 4\tau^L/3$ (c,h), $100T_f \approx 5\tau^L/3$ (d,i), and $120T_f \approx 2\tau^L$ (e,j). The panels in the upper row of the figure show the midpoints of the trajectories that belong to the clusters as given in Table I. The panels in the bottom row show noisy trajectories.

IV. CONCLUSIONS

We conducted a Lagrangian analysis in a horizontally extended turbulent Rayleigh-Bénard convection flow. The central motivation of our work was to probe the large-scale patterns in this complex three-dimensional flow, the turbulent superstructures, and compare the findings with an analysis in the complementary Eulerian frame of reference, as presented in ref. [21]. We confirm that the characteristic scales of the superstructures in the Eulerian and Lagrangian frames of reference agree. It is also shown that this characteristic time scale τ^L falls into the beginning of the Taylor regime of pair dispersion.

The Lagrangian detection of turbulent superstructures calls for an approach that studies the Lagrangian particle ensemble as a whole. This was obtained here by application of network (or graph) theory-based algorithms that were suggested in [30] and determine the spectrum of a graph Laplacian matrix $L = D - W$ in which the information on the mean mutual distance is encoded in the edge weights. The spectral gap of L indicates the number of clusters that can be determined by a standard clustering algorithm subsequently. These resulting clusters are found to agree well with the superstructure patterns, such as those of temperature shown in Fig. 4. The method works well up to time τ , whereas, notably, the FTLE field only reveals isolated ridges of strong separation for times $\ll \tau$. For longer times the dominating fraction of Lagrangian particles are decorrelated (what defines the beginning of the Taylor dispersion regime). In this case a time averaging of the Lagrangian trajectories is required in order to distinguish mixing and non-mixing trajectories. We defined therefore pseudo-trajectories. The density-based clustering algorithm DBSCAN is applied to find pseudo-trajectories that remain closely together for integration times up to 2τ . These pseudo-trajectory clusters appear to coincide with the center of circulation rolls in the Eulerian frame of reference. The clustering algorithm detects those trajectories which contribute least to the turbulent transport of heat from the bottom to the top thus forming a Lagrangian coherent set.

As we stated in the introduction, the present work is understood as a first step to work out the Lagrangian concepts to describe large-scale patterns in turbulent convection. Comprehensive parameter studies at different Prandtl numbers and for larger aspect ratios and Rayleigh numbers will be a part of the future work on this subject. This has to go in line with larger sets of trajectories. Furthermore, periodic boundary conditions in combination with variable values for the used parameters (ϵ , MinPts) will be probably necessary to advance to times at which the turbulent superstructures evolve gradually. Parts of these efforts have been started already and will be presented elsewhere.

Acknowledgments

The work of CS and AP is supported by the Priority Programme on Turbulent Superstructures of the Deutsche Forschungsgemeinschaft within Grant No. SPP 1881. JS wishes to thank the Tandon School of Engineering at New York University for financial support. We also acknowledge support with supercomputing resources by the John von Neumann Institute for Computing with project HIL12.

-
- [1] L. P. Kadanoff, Turbulent heat flow: Structures and scaling, *Phys. Today* **54**(8), 34 (2001).
 - [2] G. Ahlers, S. Grossmann, and D. Lohse, Heat transfer and large scale dynamics in turbulent Rayleigh-Bénard convection, *Rev. Mod. Phys.* **81**, 503 (2009).
 - [3] F. Chillà and J. Schumacher, New perspectives in turbulent Rayleigh-Bénard convection, *Eur. Phys. J. E* **35**, 58 (2012).
 - [4] F. Toschi and E. Bodenschatz, Lagrangian properties of particles in turbulence, *Annu. Rev. Fluid Mech.* **41**, 375 (2009).
 - [5] J. Schumacher, Lagrangian dispersion and heat transport in convective turbulence, *Phys. Rev. Lett.* **100**, 134502 (2008).
 - [6] J. Schumacher, Lagrangian studies in convective turbulence, *Phys. Rev. E* **79**, 056301 (2009).
 - [7] F. Zonta and S. Chibbaro, Entropy production and fluctuation relation in turbulent thermal convection, *Europhys. Lett.* **114**, 50011 (2016).
 - [8] M. S. Emran and J. Schumacher, Lagrangian tracer dynamics in a closed cylindrical turbulent convection cell, *Phys. Rev. E* **82**, 016303 (2010).
 - [9] H. Rajaei, P. Joshi, K. M. J. Alards, R. P. J. Kunnen, F. Toschi, and H. J. H. Clercx, Transitions in turbulent rotating convection: A Lagrangian perspective, *Phys. Rev. E* **93**, 043129 (2016).
 - [10] K. M. J. Alards, H. Rajaei, L. Del Castello, R. P. J. Kunnen, H. J. H. Clercx, and F. Toschi, Geometry of tracer trajectories in rotating turbulent flows, *Phys. Rev. Fluids* **2**, 044601 (2017).
 - [11] Y. Gasteuil, W. L. Shew, M. Gibert, F. Chillà, B. Castaing, and J.-F. Pinton, Lagrangian temperature, velocity, and local heat flux measurement in Rayleigh-Bénard convection, *Phys. Rev. Lett.* **99**, 234302 (2007).
 - [12] R. Ni, S.-D. Huang, and K.-Q. Xia, Lagrangian acceleration measurements in convective thermal turbulence, *J. Fluid Mech.* **692**, 394 (2012).
 - [13] O. Liot, A. Gay, J. Salort, M. Bourgoin, and F. Chillà, Inhomogeneity and Lagrangian unsteadiness in turbulent thermal convection, *Phys. Rev. Fluids* **1**, 064406 (2016).
 - [14] T. Hartlep, A. Tilgner, and F. H. Busse, Transition to turbulent convection in a fluid layer heated from below at moderate aspect ratio, *J. Fluid Mech.* **554**, 309 (2005).
 - [15] J. Bailon-Cuba, M. S. Emran, and J. Schumacher, Aspect ratio dependence of heat transfer and large-scale flow in turbulent convection, *J. Fluid Mech.* **655**, 152 (2010).
 - [16] M. S. Emran and J. Schumacher, Large-scale mean patterns in turbulent convection, *J. Fluid Mech.* **776**, 96 (2015).
 - [17] A. Parodi, J. von Hardenberg, G. Passoni, A. Provenzale, and E. A. Spiegel, Clustering of plumes in turbulent convection, *Phys. Rev. Lett.* **92**, 194503 (2004).
 - [18] J. von Hardenberg, A. Parodi, G. Passoni, A. Provenzale, and E. A. Spiegel, Large-scale patterns in Rayleigh-Bénard convection, *Phys. Lett. A* **372**, 2223 (2008).
 - [19] T. Hartlep, A. Tilgner, and F. H. Busse, Large scale structures in Rayleigh-Bénard convection at high Rayleigh numbers, *Phys. Rev. Lett.* **91**, 064501 (2003).
 - [20] R. A. J. M. Stevens, A. Blass, X. Zhu, R. Verzicco, and D. Lohse, Turbulent thermal superstructures in Rayleigh-Bénard convection, *Phys. Rev. Fluids* **3**, 041501(R) (2018).
 - [21] A. Pandey, J. D. Scheel, and J. Schumacher, Turbulent superstructures in Rayleigh-Bénard convection, *Nat. Commun.* **9**, 2118 (2018).
 - [22] M. R. Allshouse and T. Peacock, Lagrangian based methods for coherent structure detection, *Chaos* **25**, 097617 (2015).
 - [23] A. Hadjighasem, M. Farazmand, D. Blazevski, G. Froyland, and G. Haller, A critical comparison of Lagrangian methods for coherent structure detection, *Chaos* **27**, 053104 (2017).
 - [24] G. Froyland and K. Padberg-Gehle, Almost-invariant and finite-time coherent sets: directionality, duration, and diffusion, in W. Bahsoun, C. Bose, and G. Froyland, editors, *Ergodic Theory, Open Dynamics, and Coherent Structures*, volume 70 of *Proceedings in Mathematics and Statistics*, chapter 9, pages 171–216. Springer (2014).
 - [25] G. Haller Lagrangian coherent structures, *Ann. Rev. Fluid Mech.* **47**, 137 (2015).
 - [26] G. Haller, D. Karrasch, and F. Kogelbauer, Material barriers to diffusive and stochastic transport, *Proc. Natl. Acad. Sci. USA* **115**, 9074 (2018).
 - [27] G. Froyland, Dynamic isoperimetry and the geometry of Lagrangian coherent structures, *Nonlinearity* **28**, 3587 (2015).
 - [28] M. A. Green, C. W. Rowley, and G. Haller, Detection of Lagrangian coherent structures in 3D turbulence, *J. Fluid Mech.* **572**, 111 (2007).
 - [29] G. Froyland and K. Padberg-Gehle, A rough-and-ready cluster-based approach for extracting finite-time coherent sets from sparse and incomplete trajectory data, *Chaos* **25**, 087406 (2015).

- [30] A. Hadjighasem, D. Karrasch, H. Teramoto, and G. Haller, Spectral-clustering approach to Lagrangian vortex detection, *Phys. Rev. E* **93**, 063107 (2016).
- [31] K. L. Schlueter-Kuck and J. O. Dabiri, Coherent structure colouring: Identification of coherent structures from sparse data using graph theory, *J. Fluid Mech.* **811**, 468 (2017).
- [32] R. Banisch and P. Koltai, Understanding the geometry of transport: Diffusion maps for Lagrangian trajectory data unravel coherent sets, *Chaos* **27**, 035804 (2017).
- [33] K. Padberg-Gehle and C. Schneide, Network-based study of Lagrangian transport and mixing, *Nonlin. Processes Geophys.* **24**, 661 (2017).
- [34] F. Chung, *Spectral Graph Theory*, Oxford University Press, Oxford, 1997.
- [35] M. E. J. Newman, *Networks: An Introduction*, Oxford University Press, Oxford, 2010.
- [36] M. Ester, H.-P. Kriegel, J. Sander, X. Xu, A density-based algorithm for discovering clusters in large spatial databases with noise, *Proceedings of the Second International Conference on Knowledge Discovery and Data Mining*, AAAI Press, Portland, Oregon, pp. 226–331, 1996.
- [37] J. Shi and J. Malik, Normalized cuts and image segmentation, *IEEE Trans. Pattern Anal. Mach. Intell.* **22**, 885 (2000).
- [38] A. G. Nair and K. Taira, Network-theoretic approach to sparsified discrete vortex dynamics, *J. Fluid Mech.* **768**, 549 (2015).
- [39] K. Taira, A. G. Nair, and S. L. Brunton, Network structure of two-dimensional decaying isotropic turbulence, *J. Fluid Mech.* **795**, R2 (2016).
- [40] P. F. Fischer, An overlapping Schwarz method for spectral element solution of the incompressible Navier-Stokes equations, *J. Comp. Phys.* **133**, 84 (1997).
- [41] J. D. Scheel, M. S. Emran, and J. Schumacher, Resolving the fine-scale structure in turbulent Rayleigh-Bénard convection, *New J. Phys.* **15**, 113063 (2013).
- [42] J. D. Scheel and J. Schumacher, Local boundary layer scales in turbulent Rayleigh-Bénard convection, *J. Fluid Mech.* **758**, 344 (2014).
- [43] M. Fiedler, Algebraic connectivity of graphs, *Czech. Math.* **23**, 298 (1973).
- [44] U. von Luxburg, A tutorial on spectral clustering, *Statistics and Computing* **17**, 395 (2007).
- [45] I. Goodfellow, Y. Bengio, and A. Courville, *Deep Learning*, MIT Press, Cambridge MA, 2016.
- [46] S. A. Theerthan and J. H. Arakeri, A model for near-wall dynamics in turbulent Rayleigh-Bénard convection, *J. Fluid Mech.* **373**, 221 (1998).
- [47] B. L. Sawford, P. K. Yeung, and J. F. Hackl, Reynolds number dependence of relative dispersion statistics in isotropic turbulence, *Phys. Fluids* **20**, 065111 (2008).
- [48] W. Tang, P. W. Chan, and G. Haller, Lagrangian Coherent Structure Analysis of Terminal Winds Detected by LIDAR. Part I: Turbulence Structures, *J. Applied Meteorology and Climatology* **50**, 325 (2011).